ACS APPLIED MATERIALS & INTERFACES

Research Article

www.acsami.org

Factors Affecting the Volumetric Energy Density of Lithium-Ion Battery Materials: Particle Density Measurements and Cross-Sectional Observations of Layered $LiCo_{1-x}Ni_xO_2$ with $0 \leq x \leq 1$

Kazuhiko Mukai* and Hideyuki Nakano

Toyota Central Research and Development Laboratories, Inc., 41-1 Yokomichi, Nagakute, Aichi 480-1192, Japan

Supporting Information

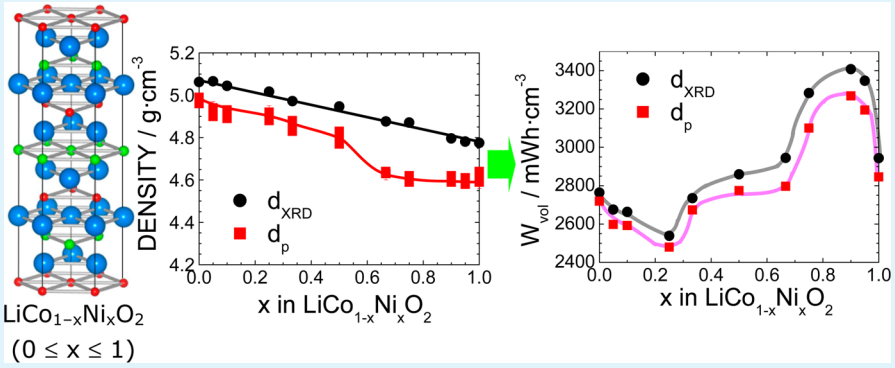

ABSTRACT: Volumetric capacity Q_{vol} (mAh cm^{-3}), more correctly, volumetric energy density W_{vol} (mWh cm^{-3}), is a crucial property of lithium-ion battery (LIB) materials, because LIBs are devices that operate in a limited space. The actual value of W_{vol} (W_{vol}^{act}) is currently limited to 40−60% of the maximum (theoretical) value of W_{vol} (W_{vol}^{max}), for reasons that have not yet been fully clarified. Thus, to gain information that will enable an increase in W_{vol}^{act} such that it is closer to W_{vol}^{max}, systematic studies of the values for Q_{vol}, W_{vol}, true density (d_{XRD}), and particle density (d_p) obtained using gas pycnometry were undertaken for $LiCo_{1-x}Ni_xO_2$ samples with $0 \leq x \leq 1$. Here, d_p is the density that includes the volume of the closed pores in the particles, and consequently is less than d_{XRD}, which is determined by X-ray diffraction (XRD) measurement. D_{XRD} monotonically decreased from 5.062(1) g cm^{-3} for $x = 0$ to 4.779(1) g cm^{-3} for $x = 1$, as expected. On the contrary, d_p decreased almost linearly from 4.98(2) g cm^{-3} for $x = 0$ to 4.80(2) g cm^{-3} for $x = 0.5$, then suddenly dropped to 4.63(2) g cm^{-3} for $x = 0.667$, and finally leveled off to a constant value (~4.6 g cm^{-3}) at larger values of x. The cross-sectional observations using a Focused Ion Beam system revealed that the significantly smaller values for d_p compared with those for d_{XRD}, particularly when $x > 0.5$, is due to the presence of closed pores in agglomerated secondary particles. This indicates that the closed pores in the secondary particles play an important role in determining the value of W_{vol}^{act} for LIBs. The formation of well-developed primary particles as a mean for increasing the value of d_p was also investigated.

KEYWORDS: *lithium insertion material, high-energy density, XRD density, focused ion beam, particle morphology, closed pore*

1. INTRODUCTION

Lithium-ion batteries (LIBs) have received significant attention as storage devices for renewable energy because of their high energy density, high power performance, and long cycle life.[1,2] For high-energy density applications, lithium insertion materials with a layered structure, such as $LiCoO_2$,[3−7] $LiNiO_2$,[8,9] and $LiCo_{1-x}Ni_xO_2$ with $0 < x < 1$,[10−14] have been employed as a positive electrode material. Here, $LiCo_{1-x}Ni_xO_2$ is a solid-solution compound between $LiCoO_2$ and $LiNiO_2$ over the entire x range, according to the monotonic change in the lattice parameters with x.[10−14] Recently, lithium insertion materials with a superlattice structure, such as $LiNi_{1/2}Mn_{1/2}O_2$ and $LiNi_{1/3}Mn_{1/3}Co_{1/3}O_2$, have been intensively investigated because of their structural stability at high voltages above 4.2 V vs Li^+/Li.[15]

The energy density (W) of a lithium insertion material is generally indicated by the gravimetric capacity (Q_{gra} (mAh g^{-1})), most likely because the theoretical gravimetric capacity (Q_{gra}^{theo}) can be easily calculated using the formula weight (M_w) and Faraday constant. For instance, Q_{gra}^{theo} = 273.84 mAh g^{-1} for $LiCoO_2$, assuming one-electron transfer per M_w of $LiCoO_2$ (= 97.8730) and 100% of Coulombic efficiency. However, because LIBs operate in a limited space, the volumetric capacity (Q_{vol} (mAh cm^{-3})), rather than Q_{gra}, is important for evaluating lithium insertion materials. The volumetric energy density (W_{vol} (mWh cm^{-3})) is given by

Received: April 13, 2014
Accepted: June 16, 2014
Published: June 16, 2014

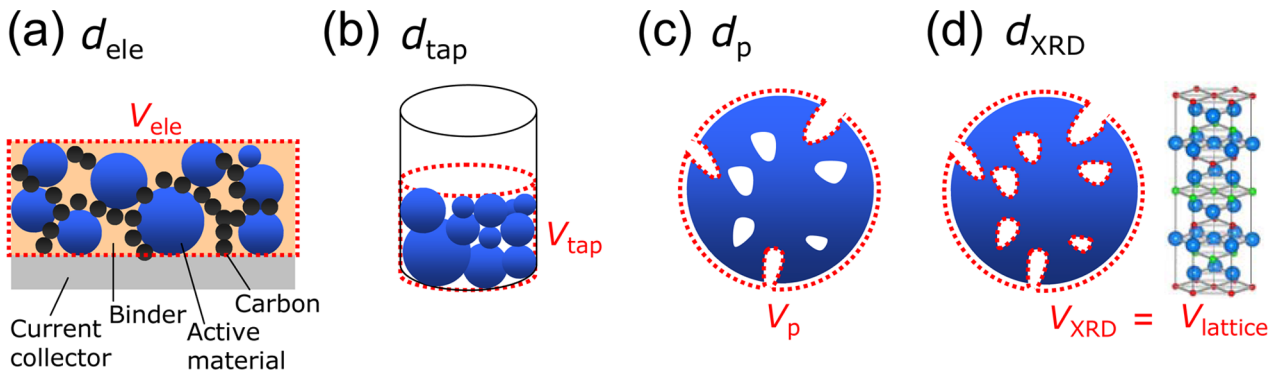

Figure 1. Definition of several densities for lithium-ion battery materials: (a) density of an electrode (d_{ele}), (b) tap density (d_{tap}), (c) particle density (d_p), and (d) density determined by X-ray diffraction (XRD) measurement (d_{XRD}). D_{ele} is the density of the active material (lithium insertion material) in the electrode volume (V_{ele}). V_{ele} contains the volumes for the conductive carbon and binder. D_{tap} is calculated using the weight of the active material and tapped volume (V_{tap}) in a container. D_{ele} and d_{tap} are strongly dependent on the experimental conditions, such as the particle size, particle shape, particle distribution of the active material, V_{tap}, and the compaction process. On the other hand, d_p and d_{XRD} are well-defined values. D_{XRD} is determined using the formula weight and lattice volume ($V_{lattice} = V_{XRD}$), whereas d_p is calculated using the volume (V_p) that includes the closed pores in a particle, which do not have contact with the particle surface. Thus, the magnitudes of the densities are in the order $d_{ele} < d_{tap} < d_p < d_{XRD}$.

$$W_{vol} = \int_0^{Q_{vol}} V dQ = V_{ave} Q_{vol} \quad (1)$$

where V_{ave} is the average operating voltage.

The maximum volumetric capacity (Q_{vol}^{max}) of a lithium insertion material is obtained using Q_{gra} and the true density, i.e., the density determined by powder X-ray diffraction (XRD) measurement (d_{XRD} (g cm^{-3})).[16] Furthermore, since V_{ave} is derived by ab initio calculations,[17] the maximum volumetric energy density (W_{vol}^{max}) can be determined. Nevertheless, it remains difficult to predict the actual volumetric capacity (Q_{vol}^{act}) or actual energy density (W_{vol}^{act}), because the actual density in the electrode (d_{ele}) is strongly affected by the particle shape, particle size, and particle distribution of the lithium insertion material. Moreover, d_{ele} is influenced by the amounts and/or types of conducting carbon and binder, which are invariably used in LIB electrodes. Although Q_{vol}^{act} (W_{vol}^{act}) is empirically known to be 40−60% of Q_{vol}^{max} (W_{vol}^{max}),[2] factors affecting the difference between d_{XRD} and d_{ele} should be clarified in order to bring Q_{vol}^{act} (W_{vol}^{act}) close to Q_{vol}^{max} (W_{vol}^{max}).

Figure 1 schematically depicts several possible density definitions for LIB materials: (a) d_{ele}, (b) tap density (d_{tap}), (c) particle density (d_p), and (d) d_{XRD}. As described above, d_{ele} is calculated using the volume of the electrode (V_{ele}) and the weight of the active material (lithium insertion material) in the electrode. D_{tap} is the density when the active material is tapped in a container with a volume V_{tap}. D_p is very close to d_{XRD}, but it is calculated using the volume (V_p) that includes the "closed" pores in a particle. Here, closed refers to pores that do not have contact with the particle surface (see Figure 1c). D_{XRD} is calculated by M_w and lattice volume $V_{lattice}$ (= V_{XRD}). The magnitudes of the different densities are in the order $d_{ele} < d_{tap} < d_p < d_{XRD}$, where the latter two densities are relatively well-defined values. Thus, as a first step, it is crucial to understand the factors affecting the difference in the values for d_p and d_{XRD}, in order to increase W_{vol}^{act}. For this purpose, a gas (expansion) pycnometer, which is used for measuring the density of polycrystalline powders, single-crystals, and liquids,[18] was employed. A liquid pycnometer was previously used to investigate the oxygen deficiency of $LiM_xMn_{2-x}O_{4-\delta}$ spinels with M = Mg, Ni, etc.[19,20] and to study the d_p of $Li(Ni_{0.8}Co_{0.1}Mn_{0.1})O_2$.[21] However, to the best of our knowledge, systematic d_p measurements associated with Q_{vol} (W_{vol}) have never been performed for lithium insertion materials.

Herein, the results of an investigation of a series of $LiCo_{1-x}Ni_xO_2$ materials with $0 \le x \le 1$, which are compounds commonly used as positive electrode materials for high-energy density LIBs,[14] are described. The x dependences of d_{XRD}, d_p, Q_{vol}, and W_{vol} were examined in order to obtain essential information required for designing advanced high-energy density LIBs. From the viewpoints of materials science, such density analyses would be important for in-depth understanding of electronic and thermal transport properties, fluid mechanics, and adsorption property of lithium transition metal oxides. This is because d_p is one of physical properties for agglomerated (macroscopic) powders, which is usually contrasted with a single (microscopic) particle based on statistical mechanics.[18] As a result, it was found that the value of d_p is significantly less than that of d_{XRD}, particularly for $x > 0.5$, because of the presence of closed pores in agglomerated secondary particles. In addition, methods for increasing the value of d_p for the composition with $x = 0.75$ were investigated.

2. EXPERIMENTAL SECTION

2.1. Sample Preparation. Polycrystalline $LiCo_{1-x}Ni_xO_2$ samples with x = 0, 0.05, 0.1, 0.25, 0.333, 0.5, 0.667, 0.75, 0.9, 0.95, and 1 were prepared using a solid-state reaction technique as reported previously.[13,14] First, Co_3O_4 and NiO powders were prepared from CoO (Kojyundo Chemical Lab. Co. Ltd.) and basic nickel carbonate (Wako Pure Chemical Industries, Ltd.), respectively, by heating at 750 °C for 12 h in air. For the samples with $x < 0.75$, Li_2CO_3 (Wako Pure Chemical Industries, Ltd.), Co_3O_4, and NiO were used as the starting materials. Each reaction mixture was well mixed using a mortar and pestle, and then pressed into a pellet with a diameter of 23 mm and a thickness of ∼5 mm. The pellet was subsequently heated in air for 12 h at 900 °C for $x \le 0.1$, 850 °C for x = 0.25 and 0.333, and 800 °C for x = 0.5 and 0.667, respectively. For the samples with $x \ge 0.75$, LiOH·H_2O (Wako Pure Chemical Industries, Ltd.), Co_3O_4, and NiO were used as the starting materials. Each pellet formed from the different reaction mixtures was preheated in an oxygen flow at 650 °C for 12 h, then ground and repressed into a pellet, and finally subjected to an oxygen flow at 750 °C for 12 h.

For the composition with x = 0.75, the samples were also prepared by a flux method using NaCl or KCl (Wako Pure Chemical Industries, Ltd.) as the reaction medium. The LiOH·H_2O/Co_3O_4/NiO mixture

and the NaCl or KCl medium were ground together using a mortar and pestle, and then heated at 750 °C in air for 18 h. The ratio of the reaction mixture to the medium was 1:3. The obtained powders were washed with distilled water and dried at 200 °C for 24 h in a vacuum.

2.2. Structural, Morphology, and Electrochemical Analyses. The crystal structure of the $LiCo_{1-x}Ni_xO_2$ samples was examined by powder XRD measurements with copper Kα radiation (RINT-2200, Rigaku Co. Ltd.) and iron Kα radiation (D8 ADVANCE, Bruker AXS, Inc.). The lattice parameters in the hexagonal setting, i.e., a_h and c_h were determined by a Rietveld analysis with RIETAN2000 software.[22] Particle morphologies were investigated by scanning electron microscopy (SEM) analyses (S-3600N, Hitachi High-Technologies Co. Ltd.). Electrochemical properties were investigated in a non-aqueous lithium cell, as reported previously.[6,7,13,14] Polyvinylidene fluoride (PVdF) dissolved in *N*-methyl-2-pyrrolidone (NMP) solution was used as the binder when preparing the mixed electrodes. A black viscous slurry consisting of 88 wt % $LiCo_{1-x}Ni_xO_2$, 6 wt % acetylene black (AB), and 6 wt % PVdF was cast on an aluminum foil with a blade to form a mixed electrode (φ = 16 mm), which was then dried under a vacuum at 120 °C for 12 h in order to evaporate NMP. A lithium metal sheet pressed on a stainless steel plate (φ = 19 mm) was used as the counter electrode. Two sheets of porous polyethylene membrane (TonenGeneral Sekiyu K. K.) were used as the separator. The electrolyte was composed of 1 M $LiPF_6$ dissolved in an ethylene carbonate/dimethyl carbonate (1/1 volume ratio) solution (Kishida Chemical Co., Ltd.). The cell was assembled in an argon-filled glovebox. The charge and discharge tests were performed in the voltage range between 3.0 and 4.2 V at a current density of 0.15 mA cm^{-2} and 25 °C.

2.3. Measurements of d_p. The d_p values were determined by gas pycnometry (Ultrapycnometer 1000, Quantachrome Instruments Inc.), which is based on the Archimedes' displacement principle.[18] With gas pycnometry, volume displacement is not measured directly but is determined using the equation of state, i.e., $PV = nRT$. First, the volume of the sample cell (V_c) and the volume of the added space (V_{add}) were calibrated using calibration spheres certified by the National Institute of Standards and Technology (NIST, 01500-NISTSM). A schematic illustration of the pycnometer system is shown in Figure S1 in the Supporting Information. Helium gas was used as the medium because it behaves as an ideal gas and penetrates pores smaller than 2 Å. Thus, the equation of state for the sample cell is represented by

$$P_a V_c = n_c R T_a \tag{2}$$

and for the added space, it is as follows

$$P_a V_{add} = n_{add} R T_a \tag{3}$$

where P_a is the ambient pressure (~101 kPa), n_c and n_{add} are the moles of helium gas in the sample cell and the added space, respectively, R is the gas constant, and T is the ambient temperature (= 25 ± 0.5 °C). When a $LiCo_{1-x}Ni_xO_2$ sample is placed in the sample cell, the equation of state for the sample cell can be described as

$$P_a(V_c - V_s) = n_1 R T_a \tag{4}$$

where V_s is the volume of the sample, and n_1 is the moles of remaining the helium gas. The weight of the $LiCo_{1-x}Ni_xO_2$ (w_s) samples in this study was ~1.8 g for all measurements. The sample cell was then pressurized to P_2 (~138 kPa)

$$P_2(V_c - V_s) = n_2 R T_a \tag{5}$$

where n_2 is the remaining moles of helium gas at P_2. When the valve between V_c and V_{add} was opened, the pressure dropped to an equilibrium value of P_3

$$P_3(V_c - V_s + V_{add}) = n_2 R T_a + n_{add} R T_a. \tag{6}$$

Using eqs 3 and 5, V_s was determined as

$$V_s = V_c + \frac{V_a}{\left(1 - \frac{P_2 - P_a}{P_3 - P_a}\right)} = V_c + \frac{V_a}{\left(1 - \frac{P_2}{P_3}\right)} \tag{7}$$

and finally, the value for d_p (= w_s/V_s) was obtained. Therefore, it is possible to determine the value of d_p with just one measurement. However, in order to obtain a reliable d_p value, the measurement was repeated 100 times for each sample. That is, after one d_p measurement, the sample cell was repressurized to P_2, the valve between V_c and V_{add} was opened again, and V_s (d_p) was calculated. The averaged d_s value for each sample was determined using the data for the last 50 measurements. The d_p value for x = 0 as a function of each measurement is shown in Figure S2 of the Supporting Information. In addition, at least three independent runs were performed for each $LiCo_{1-x}Ni_xO_2$ sample in order to confirm the reproducibility of the obtained d_p values.

2.4. Cross-Sectional Observations. Cross-sectional views of the $LiCo_{1-x}Ni_xO_2$ electrodes were observed using a focused ion beam (FIB) system with FB-2000 (Hitachi High-Tech Science Systems Co.). The electrodes consisted of 88 wt % $LiCo_{1-x}Ni_xO_2$, 6 wt % AB, and 6 wt % PVdF. Three ranges of Ga^+ ion currents were applied in order to cut the electrodes: 20 nA for 100 min, 2.6 nA for 30 min, and 0.62 nA for 10 min. The dimensions of the cutting zone were approximately 30 μm in width, 50 μm in height, and 5 μm in depth. After cutting, each electrode was tilted ~90°, and then the cross section of the electrode was observed using Ga^+-induced SEM. During SEM observation, the Ga^+-ion current was maintained at 0.15 nA in order to avoid possible beam damage. The Ga^+ ions were accelerated at 30 kV under a vacuum of ~1 × 10^{-4} Pa.

3. RESULTS AND DISCUSSION

3.1. Crystal Structure. Figure 2 shows the XRD patterns for the $LiCo_{1-x}Ni_xO_2$ samples with (a) x = 0, (b) x = 0.25, (c) x = 0.5, (d) x = 0.75, and (e) x = 1. The XRD patterns for the other $LiCo_{1-x}Ni_xO_2$ samples, i.e., x = 0.05, 0.1, 0.333, 0.667, 0.9, and 0.95, are shown in Figure S3 of the Supporting Information. The XRD patterns with the $x \geq 0.75$ samples were identified as a single-phase of a layered structure with the $R\bar{3}m$ space group, in which the Li^+ ions occupy the octahedral 3*b* site, whereas the Co^{3+} (Ni^{3+}) ions occupy the octahedral 3*a* site. For the samples with $x \geq 0.9$, the Rietveld analysis with RIETAN2000[22] clarified the presence of a small amount of Ni ions in the 3*b* (Li) site; more specifically, z in $(Li_{1-z}Ni_z)_{3b}[Co_{1-x}Ni_{x-z}]_{3a}O_2$ is 0.01(1) for x = 0.9, 0.02(1) for x = 0.95, and 0.03(1) for x = 1. Results of the Rietveld

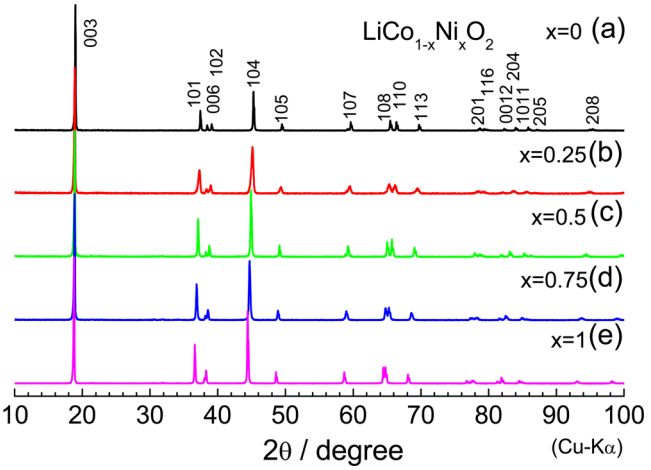

Figure 2. XRD patterns of the $LiCo_{1-x}Ni_xO_2$ samples with (a) x = 0, (b) x = 0.25, (c) x = 0.5, (d) x = 0.75, and (e) x = 1.

dx.doi.org/10.1021/am502242z | ACS Appl. Mater. Interfaces 2014, 6, 10583−10592

analysis are shown in Figure S4 of the Supporting Information. Figure 3a shows the lattice parameters for the a_h- and c_h-axes,

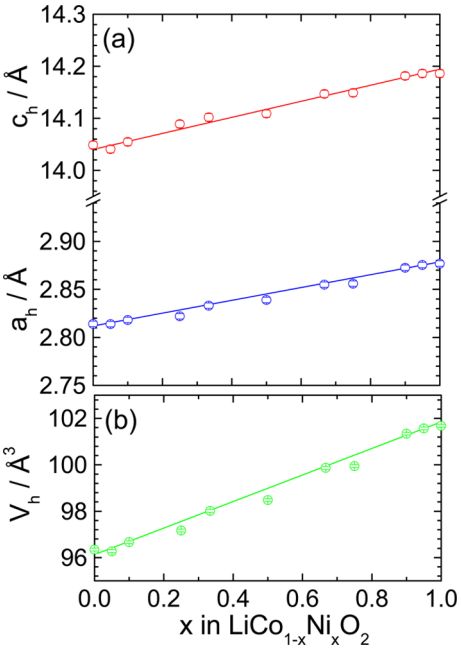

Figure 3. (a) Lattice parameters for the a_h- and c_h-axes and (b) unit-cell volume V_h for the $LiCo_{1-x}Ni_xO_2$ samples with $0 \le x \le 1$. The values of a_h and c_h values were determined by the Rietveld analyses.

respectively, as a function of x in $LiCo_{1-x}Ni_xO_2$. Both a_h and c_h increases with the value of x, indicating that the Co and Ni ions are homogeneously distributed in the Co/Ni layers over the entire range of x values. The increase in a_h and c_h with x is understood by the increase in the ionic radius (r) resulting when Co^{3+} ions are replaced with Ni^{3+} ions. That is, when the coordination number is six for both ions, r = 0.53 Å for the Co^{3+} ions in a low-spin state ($t_{2g}^6e_g^0$), whereas r = 0.56 Å for the Ni^{3+} ions in a low-spin state ($t_{2g}^6e_g^1$).[23]

Due to the linear relationship between a_h (c_h) and x, the variation of the unit cell volume V_h also exhibits a monotonic change with x (Figure 3b). Therefore, the structural parameters of the $LiCo_{1-x}Ni_xO_2$ samples prepared in this study, which are summarized in Table 1, are consistent with the previous results reported for $LiCo_{1-x}Ni_xO_2$.[10−14]

3.2. Electrochemical Properties. Figure 4 presents the charge and discharge curves for the $Li/LiCo_{1-x}Ni_xO_2$ cells with

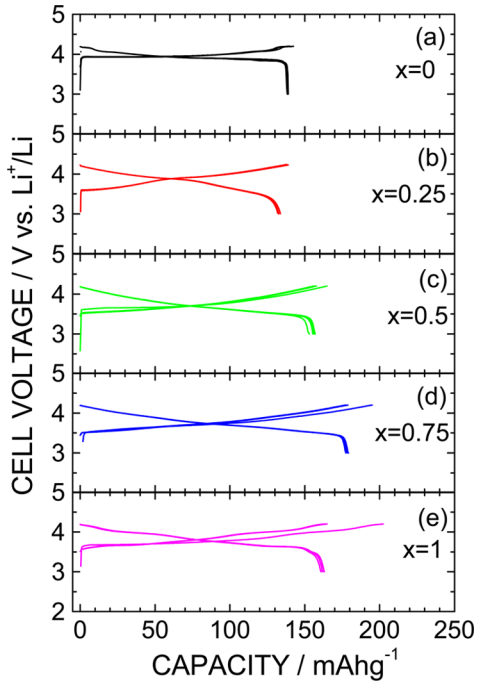

Figure 4. Charge and discharge curves for the $Li/LiCo_{1-x}Ni_xO_2$ cells with (a) x = 0, (b) x = 0.25, (c) x = 0.5, (d) x = 0.75, and (e) x = 1. The cells were operated in the voltage range between 3.0 and 4.2 V at a current density of 0.15 mA cm^{-2} and 25 °C.

(a) x = 0, (b) x = 0.25, (c) x = 0.5, (d) x = 0.75, and (e) x = 1. The charge and discharge curves for the $Li/LiCo_{1-x}Ni_xO_2$ cells with x = 0.05, 0.1, 0.333, 0.667, 0.9, and 0.95 can be seen in Figure S5 of the Supporting Information. All of the cells were operated in the voltage range between 3.0 and 4.2 V at a current density of 0.15 mA cm^{-2} and 25 °C. The charge cutoff voltage was restricted to 4.2 V, in order to avoid capacity fading due to the inherent structural phase transitions of $LiCoO_2$[4−7] and $LiNiO_2$,[8,9] and/or degradation of the electrolytes at high voltages. For the x = 0 sample, the cell voltage (V_{cell}) initially

Table 1. Structural Parameters of a_h, c_h, and V_h, Densities of d_{XRD} and d_p, Capacities of Q_{gra} and Q_{vol}, and Energy Densities of W_{gra} and W_{vol} for the $LiCo_{1-x}Ni_xO_2$ Samples with $0 \le x \le 1$

	structural parameters		density			capacity and energy density		
x	lattice parameters (Å)	lattice volume (Å^3)	d_{XRD} (g cm^{-3})	d_p (g cm^{-3})	Q_{gra} (mAh g^{-1})	W_{gra} (mWh g^{-1})	Q_{vol}[a] (mAh cm^{-3})	W_{vol}[a] (mWh cm^{-3})
0	a_h = 2.814(1), c_h = 14.05(1)	96.34(1)	5.062(1)	4.98(2)	139	546	692	2720
0.05	a_h = 2.814(1), c_h = 14.04(1)	96.27(1)	5.066(1)	4.92(2)	135	528	664	2598
0.1	a_h = 2.818(1), c_h = 14.05(1)	96.67(1)	5.044(1)	4.91(2)	135	528	663	2592
0.25	a_h = 2.822(1), c_h = 14.09(1)	97.17(1)	5.017(1)	4.90(2)	133	506	652	2479
0.333	a_h = 2.833(1), c_h = 14.10(1)	98.02(1)	4.972(1)	4.86(2)	146	550	710	2673
0.5	a_h = 2.839(1), c_h = 14.11(1)	98.48(1)	4.947(1)	4.80(2)	156	578	749	2774
0.667	a_h = 2.855(1), c_h = 14.15(1)	99.86(1)	4.876(1)	4.63(2)	162	604	751	2797
0.75	a_h = 2.856(1), c_h = 14.15(1)	99.95(1)	4.871(1)	4.60(2)	179	674	823	3100
0.9	a_h = 2.873(1), c_h = 14.18(1)	101.3(1)	4.806(1)	4.61(2)	186	709	858	3268
0.95	a_h = 2.875(1), c_h = 14.19(1)	101.6(1)	4.809(1)	4.59(2)	183	696	840	3194
1	a_h = 2.877(1), c_h = 14.19(1)	101.7(1)	4.779(1)	4.62(2)	161	616	739	2846

[a]The values of Q_{vol} and W_{vol} were calculated using the d_p value.

dx.doi.org/10.1021/am502242z | ACS Appl. Mater. Interfaces 2014, 6, 10583−10592

increases rapidly from ~3.0 V, and then keeps nearly constant at ~3.9 V up to $Q_{gra} \approx 70$ mAh g^{-1}. The constant operating voltage of ~3.9 V corresponds to the formation of two $R\bar{3}m$ phases, which is characteristics for stoichiometric $LiCoO_2$.[4−7] As x increases from 0 to 0.25, the operating voltage at the beginning of the charge reaction decreases to ~3.6 V (see Figures 4b and Figure S5 in the Supporting Information), indicating that the Ni^{3+} ions are oxidized before the Co^{3+} ions.[12] For the $0.333 \leq x \leq 0.75$ samples, the V_{cell} almost monotonically increases with Q_{gra}, suggesting a one-phase reaction; in other words, no structural phase change occurs during the charge and discharge reactions. For the $x \geq 0.9$ samples, however, plateaus are observed at around 3.6, 4.0, and 4.2 V. The former two plateaus suggest the formation and annihilation of a monoclinic ($C2/m$) phase, respectively, whereas the last plateau indicates the formation of two $R\bar{3}m$ phases in delithiated Li_yNiO_2 with $y < 0.5$.[8,9,13,14]

In Figure 5a, the values for Q_{gra} for the $LiCo_{1-x}Ni_xO_2$ samples are plotted as a function of x. The values for Q_{gra} in the figure are the discharge capacities for the second cycle, as shown in Figure 4 and Figure S5 in the Supporting Information. The x dependence of Q_{gra} can be divided into three distinct regions; (i) $0 \leq x \leq 0.25$, (ii) $0.25 < x < 0.75$, and (iii) $x \geq 0.75$. In region (i), Q_{gra} slightly decreases from 139 mAh g^{-1} to 133 mAh g^{-1}, while in region (ii), Q_{gra} increases with a change in the slope (dQ_{gra}/dx) and approaches 162 mAh g^{-1} for $x = 0.667$. Finally, in region (iii), Q_{gra} rapidly increases from $x = 0.75$ and reaches a maximum (= 186 mAh g^{-1}) for the $x = 0.9$ sample, and then declines to 161 mAh·g^{-1} when $x = 1$. In our previous magnetic and electrochemical studies of $LiCo_{1-x}Ni_xO_2$ with $x \geq 0.75$, a similar x dependence was observed in region (iii), although in that case, Q_{gra} = 206 mAh g^{-1} for $x = 0.9$, Q_{gra} = 217 mAh g^{-1} for $x = 0.95$, and Q_{gra} = 180 mAh g^{-1} for $x = 1$.[14] The difference in the values for Q_{gra} obtained in this and previous studies is attributed to the difference in the z amounts in $(Li_{1-z}Ni_z)_{3b}[Co_{1-x}Ni_{x-z}]_{3a}O_2$,[14] as described below. The increase in Q_{gra} with x can be explained by a decrease in the redox potentials below 4.2 V with x.[24] Although there are three major redox potentials at 3.91, 4.18, and 4.50 V for $x = 0$, the former two redox potentials are decreased to 3.58 and 4.05 V when $x = 0.5$ because of the formation of the Ni^{3+}/Ni^{4+} redox couple.[24] In region (iii), z also contributes to Q_{gra}. Because the presence of z disturbs the diffusion of Li^+ ions in the Li layer, electrochemical properties, such as Q_{gra} and irreversible capacity, strongly depend on the quantity of z, as reported previously.[9−14] Indeed, as clarified by the Rietveld analysis (Section 3.1), the values of z for the x = 0.9 and 0.95 samples are smaller than that for the $x = 1$ sample. Thus, the Ni^{3+}/Ni^{4+} redox couple and the quantity of z in $(Li_{1-z}Ni_z)_{3b}[Co_{1-x}Ni_{x-z}]_{3a}O_2$ mainly determine the values of Q_{gra}, which was measured in the voltage range between 3.0 and 4.2 V.

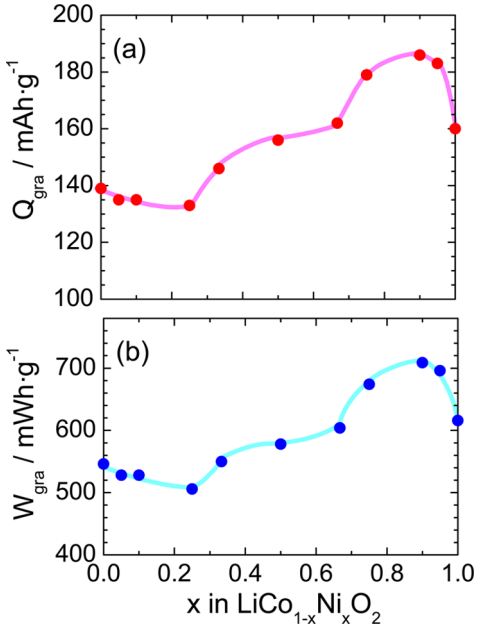

Figure 5. (a) Gravimetric discharge capacity (Q_{gra}) and (b) gravimetric energy density (W_{gra}) as a function of x in $LiCo_{1-x}Ni_xO_2$. Q_{gra} is the discharge capacity for the 2nd cycle shown in Figure 4 and Figure S5 in the Supporting Information. W_{gra} was obtained by multiplying Q_{gra} by the average operating voltage (V_{ave}).

The W_{gra} value is then obtained by multiplying Q_{gra} and V_{ave}. As shown in Figure S6 in the Supporting Information, the value of V_{ave} is minimal for the $x = 0.5$ sample. That is, V_{ave} = 3.93, 3.71, and 3.80 V for the x = 0, 0.5, and 1 samples, respectively. However, since the difference in V_{ave} for $x = 0$ and 0.5 is within ~6%, it can be concluded that V_{ave} does not strongly affect W_{gra} for $LiCo_{1-x}Ni_xO_2$. In fact, the x dependence of W_{gra} is quite similar to that of Q_{gra} (Figure 5b); as x increases from 0 to 0.25, W_{gra} slightly decreases from 546 mWh g^{-1} to 506 mWh g^{-1}, then increases with further increasing x, and finally reaches a maximum (= 709 mWh g^{-1}) for $x = 0.9$. The values of Q_{gra} and W_{gra} for the $LiCo_{1-x}Ni_xO_2$ samples are listed in Table 1.

3.3. d_p Measurements. Figure 6a shows the values of d_p and d_{XRD} for the $LiCo_{1-x}Ni_xO_2$ samples. The d_p and d_{XRD} values are also summarized in Table 1, where d_p is the average of three independent runs. The d_{XRD} value almost linearly decreases with increasing x; d_{XRD} = 5.062(1), 4.947(1), and 4.779(1) g cm^{-3} for the x = 0, 0.5, and 1 samples, respectively. The

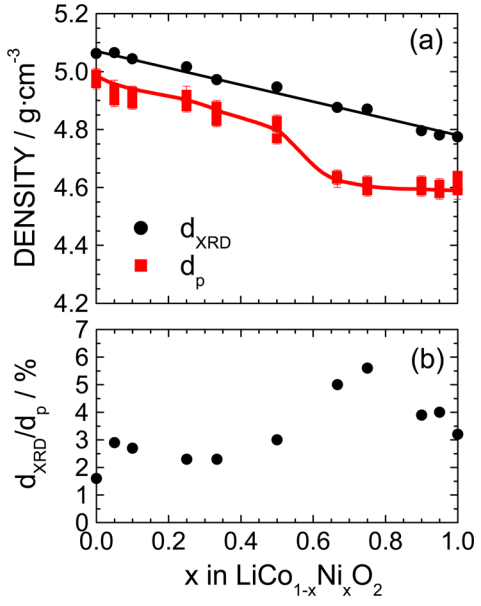

Figure 6. (a) Particle density (d_p) and true density (d_{XRD}) as a function of x in $LiCo_{1-x}Ni_xO_2$. D_{XRD} was determined by the XRD measurements. (b) The difference between d_p and d_{XRD}, i.e., the d_{XRD}/d_p ratio.

dx.doi.org/10.1021/am502242z | ACS Appl. Mater. Interfaces 2014, 6, 10583−10592

decrease in d_{XRD} with x is due to the increase in V_h with x (see Figure 3b), because M_w for $LiCoO_2$ (= 97.8730) is close to that for $LiNiO_2$ (= 97.6332). On the contrary, the x dependence of d_p is not monotonic. As x increases from 0 to 0.5, d_p almost decreases linearly from 4.98(2) g cm^{-3} to 4.80(2) g cm^{-3}, then suddenly drops to 4.63(2) g cm^{-3} for x = 0.667, and finally levels off at a constant value (~4.6 g cm^{-3}) as x increases further. As can be seen in Figure 6b, the difference between d_{XRD} and d_p, i.e., the d_{XRD}/d_p ratio, has a minimum value at x = 0 (= 1.6%). Then, the d_{XRD}/d_p is almost constant (~3.0%) until x = 0.5, and finally has a maximum (= 6%) for x = 0.75. As illustrated in Figure 1c, d_p is the density that includes the volume of the closed pores in the particles. Hence, the large difference in the values for d_{XRD} and d_p for the samples with x > 0.5 indicates the presence of closed pores in the particles. A detailed analysis for such difference is presented in the Section 3.4.

Figure 7 shows the values of (a) Q_{vol}, (b) W_{vol}, and (c) $W_{vol}(d_p)/W_{vol}(d_{XRD})$ for the $LiCo_{1-x}Ni_xO_2$ samples, where the

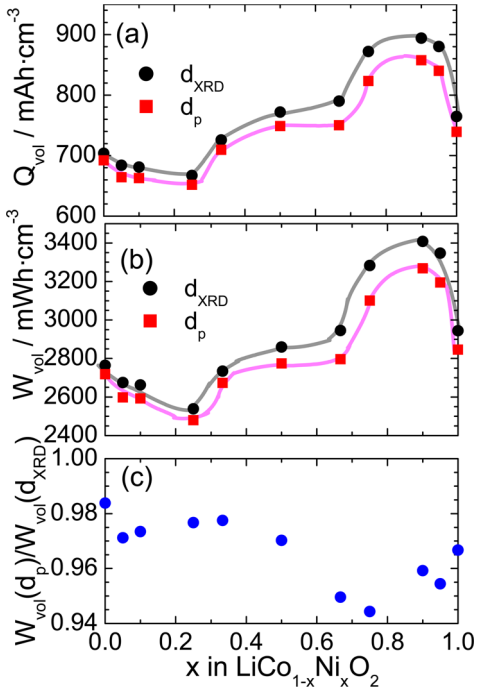

Figure 7. (a) Volumetric discharge capacity (Q_{vol}), (b) volumetric energy density (W_{vol}), and (c) the ratio of $W_{vol}(d_p)/W_{vol}(d_{XRD})$ as a function of x in $LiCo_{1-x}Ni_xO_2$. Note that the $W_{vol}(d_p)/W_{vol}(d_{XRD})$ ratio is exactly same to the $Q_{vol}(d_p)/Q_{vol}(d_{XRD})$ ratio, because the $W_{vol}(d_p)$ and $W_{vol}(d_{XRD})$ values are calculated by $W_{vol}(d_p) = Q_{vol}(d_p) V_{ave}$ and $W_{vol}(d_{XRD}) = Q_{vol}(d_{XRD})V_{ave}$, respectively.

Q_{vol} and W_{vol} were calculated using both d_{XRD} and d_p values. The x dependence of Q_{vol} calculated using d_{XRD} is similar to that of Q_{gra} (see Figure 5 b); as x increases from 0, Q_{vol} slightly decreases in region (i), then increases with a change in the slope (dQ_{vol}/dx) in region (ii), and finally has a maximum at x = 0.9 in region (iii). The maximum and minimum Q_{vol} values are 894 mAh cm^{-3} for x = 0.9 and 652 mAh cm^{-3} for x = 0.25, respectively. At these compositions, the Q_{gra} values also have the maximum and minimum values, i.e., 186 mAh g^{-1} for x = 0.9 and 133 mAh g^{-1} for x = 0.25 (Figure 5a and Table 1). However, the $Q_{vol}(min)/Q_{vol}(max)$ ratio is smaller than the $Q_{gra}(min)/Q_{gra}(max)$ ratio, because d_{XRD} monotonically decreases with x. For the Q_{vol} values calculated using d_p, the differences between the samples are smaller because of the large decrease in the values for d_p compared to those for d_{XRD}, particularly for the samples with x > 0.5. As a result, the maximum and minimum Q_{vol} values obtained using d_p are 858 mAh cm^{-3} for x = 0.9 and 652 mAh cm^{-3} for x = 0.25, respectively.

As can be seen in Figure 7b, the x dependence of W_{vol} is essentially similar to that of Q_{vol}. The value for W_{vol} obtained using d_{XRD} (d_p) decreases from 2764 (2720) mWh cm^{-3} at x = 0 to 2540 (2479) mWh cm^{-3} at x = 0.25, then increases to 2945 (2797) mWh cm^{-3} at x = 0.667, and finally reaches a maximum of 3407 (3268) mWh cm^{-3} at x = 0.9. It should be noted that the difference in the values of W_{vol} calculated using d_{XRD} and d_p is ~1.6% at x = 0 and ~4.3% at x = 0.75. This variation suggests that W_{vol}^{act} (Q_{vol}^{act}) for the x = 0.75 sample is less than that for the x = 0 sample, because of the larger difference in the values for d_{XRD} and d_p. For the same reason, the $W_{vol}(d_p)/W_{vol}(d_{XRD})$ ratio has the minimum at the x = 0.75 composition (see Figure 7c). Note that the $W_{vol}(d_p)/W_{vol}(d_{XRD})$ ratio is exactly same to the $Q_{vol}(d_p)/Q_{vol}(d_{XRD})$ ratio, because the $W_{vol}(d_p)$ and $W_{vol}(d_{XRD})$ values are calculated by $W_{vol}(d_p) = Q_{vol}(d_p) \times V_{ave}$ and $W_{vol}(d_{XRD}) = Q_{vol}(d_{XRD}) \times V_{ave}$, respectively.

3.4. Cross-Sectional Observations. To clarify the origin of the significantly smaller values for d_p as compared to d_{XRD}, particularly when x > 0.5, cross-sectional views of the samples were obtained, and the results are shown in Figure 8: (a) x = 0, (b) x = 0.75, and (c) x = 1. The primary particles in the x = 0

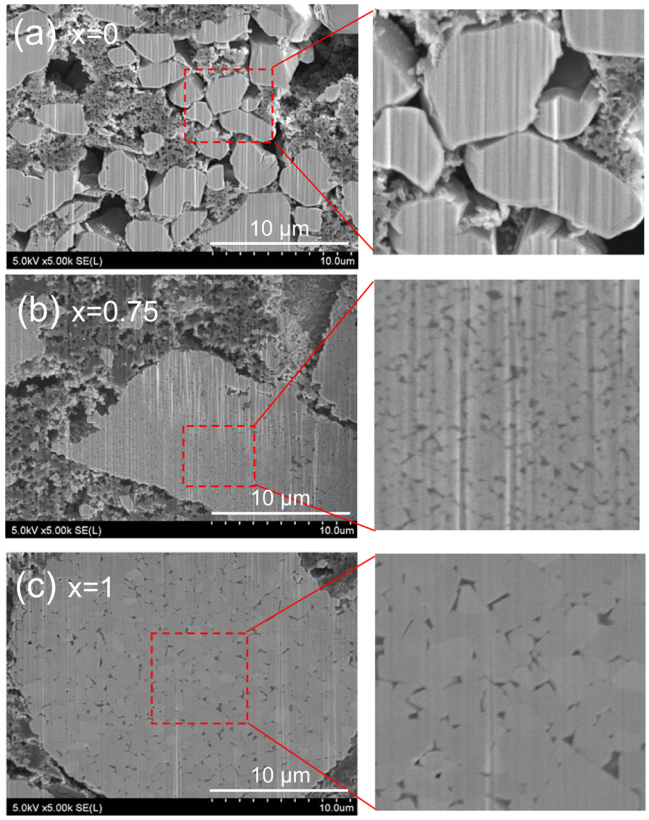

Figure 8. Cross-sectional views for the $LiCo_{1-x}Ni_xO_2$ samples with (a) x = 0, (b) x = 075, and (c) x = 1. Enlarged cross-sectional views are also shown to clarify the existence/absence of closed pores and grain boundaries in the particles.

sample are separated from one another, and their average size is approximately 3 μm. In addition, neither grain boundaries nor closed pores are observed in these primary particles, as can be seen in the enlarged cross-sectional view of Figure 8a. On the contrary, for the x = 0.75 sample, the primary particles located within ~0.3 μm are agglomerated together, forming large secondary particles of ~20 μm. Furthermore, as can be clearly seen in the enlarged cross-sectional view of Figure 8b, many closed pores exist in the secondary particles. Thus, the significantly smaller value for d_p compared to that of d_{XRD} can be attributed to the presence of closed pores in the secondary particles, because the value of d_p does not include these volumes (Figure 1c). For the x = 1 sample, the situation is similar to that for the x = 0.75 sample; however, the size of the closed pores appears to be larger than that for the x = 0.75 sample (see the enlarged cross-sectional view of Figure 8c). This suggests that the average size of the primary particles for the x = 1 sample (~1 μm) is larger than that for the x = 0.75 sample.

The presence of closed pores unambiguously reduces the value of W_{vol}^{act} (Q_{vol}^{act}) for $LiCo_{1-x}Ni_xO_2$. Moreover, it leads to possible capacity fading, especially for high-rate charge and discharge tests, because electrical conduction is only achieved from the surfaces of secondary particles. That is, if each primary particle is isolated from other primary particles due to a change in a_h, c_h, or V_h, the electrical isolation of the active primary particles occurs. The advantages of cross-sectional observations using FIB rather than conventional SEM analyses should also be emphasized. Although our recent SEM observations of stoichiometric $LiCoO_2$ indicated agglomerated particle morphology,[7] the cross-sectional views shown in Figure 8a clarified that the primary particles for the x = 0 sample are distinct from one another. It should be also noted that that conducting carbon and binder are added when forming mixed electrodes. Thus, the observations of not only active materials but also mixed electrodes are essential for elucidating the distribution of the active materials.

The agglomerated particle morphology described above is characteristic of Ni-rich $LiCo_{1-x}Ni_xO_2$ compounds, as reported for $Li(Co_{0.1}Ni_{0.8}Mn_{0.1})O_2$[21] and $LiCo_{0.15}Ni_{0.82}Al_{0.03}O_2$.[25] With respect to the sample with x = 0 ($LiCoO_2$) and Ni-rich $LiCo_{1-x}Ni_xO_2$ compounds, there are several possibilities for the origin of the morphological differences. One of the most probable factors is the synthesis temperature. $LiCoO_2$ is typically prepared at 900 °C in order to obtain a highly crystallized material. However, for Ni-rich $LiCo_{1-x}Ni_xO_2$ compounds, high temperature synthesis above 750 °C inevitably induces the formation of a rock-salt phase $(Li_{1-z}Ni_z)_{3b}[Co_{1-x}Ni_{x-z}]_{3a}O_2$ ($Fm\bar{3}m$) with z > ~0.1, which is electrochemically inactive.[9−11] Thus, the synthesis temperature for Ni-rich $LiCo_{1-x}Ni_xO_2$ materials is typically limited to ~750 °C,[9,13,14] and consequently, is not sufficient for obtaining well-developed primary particles. In this study, a synthesis temperature of 750 °C was employed for the samples with $x \geq$ 0.75. The nearly linear x dependence in d_p can also be explained by the synthesis temperature. A second factor is the surface energy. $LiCoO_2$, particularly when prepared in a flux medium,[26] exhibits a hexagonal shape because of the anisotropic crystal growth along the [00l] direction, whereas $LiNiO_2$ and its derivatives exhibit nonuniform particle morphologies.[21,25] As pointed out by Kim and co-workers,[21,25] this difference implies that the surface energy of $LiNiO_2$ is less than that of $LiCoO_2$. Further theoretical studies on surface energy on $LiCo_{1-x}Ni_xO_2$ with x would provide useful information for determining the particle morphology of $LiCo_{1-x}Ni_xO_2$.

3.5. Attempt to Increasing d_p. The cross-sectional observations of the electrodes revealed that significantly smaller value for d_p as compared with d_{XRD}, particularly for the samples with x > 0.5, was due to the presence of closed pores in agglomerated secondary particles. Therefore, an attempt was made to increase d_p for the x = 0.75 sample, because the value of d_{XRD}/d_p reached the maximum for this composition (Figure 6b). One approach for obtaining high d_p values is to synthesize well-developed primary particles, such as those observed for the x = 0 sample (Figure 8a). For this purpose, the flux method using NaCl or KCl as the medium was employed, as reported for $Li(Ni_{0.8}Co_{0.1}Mn_{0.1})O_2$,[21] $LiCoO_2$,[26] and $Li[Li_{1/3}Ti_{5/3}]O_4$.[27] Such compounds were typically heated at 900−1000 °C,[21,26,27] because the melting points of NaCl and KCl are 800 and 770 °C, respectively. However, in this study, the heating temperature was restricted to 750 °C in order to minimize the value of z in $(Li_{1-z}Ni_z)_{3b}[Co_{1-x}Ni_{x-z}]_{3a}O_2$.

As expected, the x = 0.75 samples prepared using NaCl or KCl as a flux medium have greater d_p values compared to that for the conventional x = 0.75 sample; d_p = 4.85(4) and 4.78(4) g cm^{-3} for NaCl and KCl, respectively, while d_p = 4.60(2) g cm^{-3} for the conventional x = 0.75 sample. These values are very close to the d_{XRD} value (= 4.871(1) g cm^{-3}) for the conventional x = 0.75 sample (Figure 6a and Table 1). Figure 9

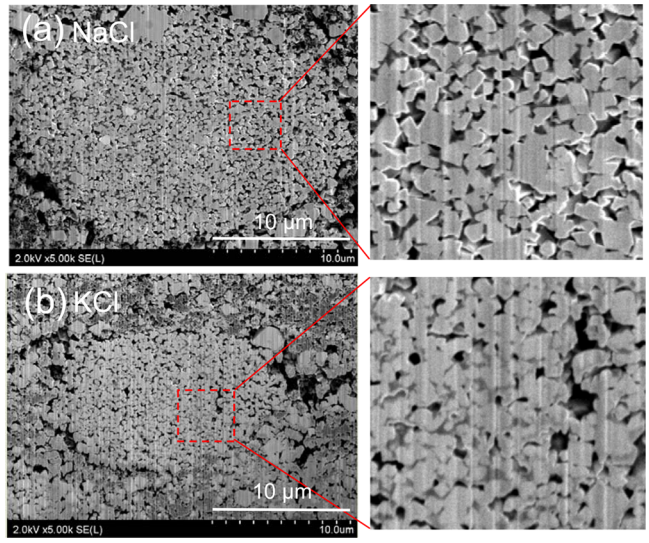

Figure 9. Cross-sectional views for the $LiCo_{1-x}Ni_xO_2$ samples with x = 0.75 prepared in (a) NaCl and (b) KCl media. The samples were synthesized by heating the reaction mixtures at 750 °C in air for 18 h. Enlarged cross-sectional views are also shown to clarify the existence/absence of closed pores and grain boundaries in the particles.

shows the cross-sectional views for the x = 0.75 samples prepared using (a) NaCl and (b) KCl as a flux medium. The primary particles prepared using flux media, with an average size of ~0.5 μm, are larger than those for the conventional x = 0.75 sample (< ~ 0.3 μm). However, the primary particles are not as developed as those in the x = 0 sample (Figure 8a), and are still agglomerated, forming large secondary particles (~25 μm for NaCl and ~20 μm for KCl). It can be also clearly seen in Figures 9a and 9b that each type of primary particles is distributed in a more separate form, compared to those of the conventional x = 0.75 and 1 samples (Figure 8b, c,

respectively). Thus, opened, rather than closed, pores in the secondary particles are considered to contribute to higher d_p values.

Next, we performed the XRD measurements on the $x = 0.75$ samples prepared using the NaCl and KCl flux media by iron Kα radiation. Figure 10 shows the results of Rietveld analyses

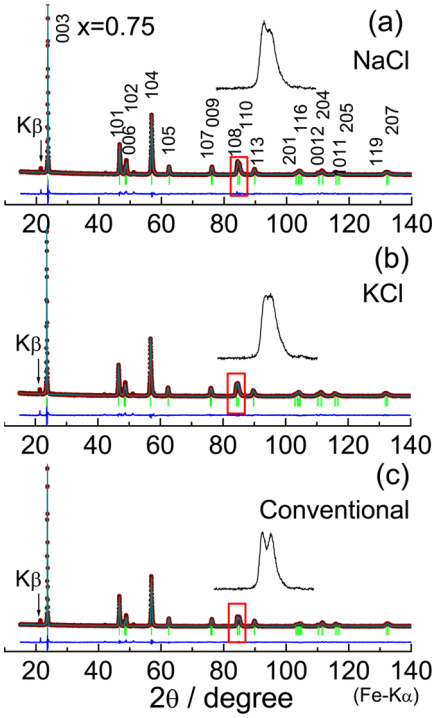

Figure 10. Results of the Rietveld analyses for the $LiCo_{1-x}Ni_xO_2$ samples with $x = 0.75$ prepared in (a) NaCl and (b) KCl media. (c) Result for the conventional $x = 0.75$ sample shown for comparison. Enlarged XRD patterns at approximately $2\theta = 85°$ are shown in the inset. The diffraction line indicated by arrow is due to the iron Kβ radiation.

for the samples prepared using (a) NaCl and (b) KCl as flux media. The result of Rietveld analysis for the conventional $x = 0.75$ sample is also shown in c for comparison. The crystal structure of both a and b is assigned as a single-phase with layered structure with the $R\bar{3}m$ space group. Impurity phases, including Co_3O_4 and/or NiO, are barely detected in both XRD patterns, where $d_{XRD} = 6.11$ g cm^{-3} for Co_3O_4 and $d_{XRD} = 6.67$ g cm^{-3} for NiO. The lattice parameters are calculated as $a_h = 2.871(1)$ Å and $c_h = 14.15(1)$ Å for (a), and $a_h = 2.871(1)$ Å and $c_h = 14.16(1)$ Å for (b), which are similar to those for the conventional $x = 0.75$ sample (Table 1). However, the integrated peak ratio for the 003 and 104 diffraction lines $I(003)/I(104)$ is clearly different between the samples prepared using the flux media and the conventional sample. The $I(003)/I(104)$ values are 1.00, 1.02, and 1.72 for the NaCl, KCl, and conventional $x = 0.75$ samples. This result suggests that, as reported previously,[9−14] a large amount of z exists in $(Li_{1-z}Ni_z)_{3b}[Co_{1-x}Ni_{x-z}]_{3a}O_2$ samples prepared by the flux method. Indeed, the Rietveld analyses revealed that $z = 0.06(1)$ for NaCl and $z = 0.05(1)$ for KCl, but $z \approx 0$ for the conventional $x = 0.75$ sample. The enlarged XRD patterns at approximately $2\theta = 85°$ also provide another insight into the crystal structure. For the samples prepared using NaCl and KCl media, the 108 diffraction line is located near the 110 diffraction line, while, for the conventional $x = 0.75$ sample, the 108 and 110 diffraction lines are clearly separated from one another. According to the structural relationship between cubic and hexagonal systems, the 440 diffraction line of the cubic system is converted to the 108 and 110 diffraction lines of the hexagonal system, when $c_h/a_h \neq 2\sqrt{6}$ (~4.90).[12] Therefore, it can be concluded that the synthesis by the flux method using NaCl or KCl medium induces a structural change from the hexagonal phase to the cubic phase, simultaneously, although such method provides high d_p values at the $x = 0.75$ composition.

It should be noted that both phenomena (high d_p value and structural change) are also observed for the $Li(Ni_{0.8}Co_{0.1}Mn_{0.1})O_2$ compound, which was prepared using the NaCl flux medium at 900 °C.[21] That is, the d_p value of such compound is 4.83 g cm^{-3},[21] which is slightly higher than the expected d_{XRD} value (~4.81 g cm^{-3} or less, because the substitution of Mn ions for Co ions decreases M_w). Moreover, the XRD measurements indicated the cubic structural character; the peak intensity of the 003 diffraction line is almost similar to that of the 104 diffraction line, and the 108 and 110 diffraction lines are not clearly separated.[21]

Considering from the previous results on the $(Li_{1-z}Ni_z)_{3b}[Co_{1-x}Ni_{x-z}]_{3a}O_2$ compounds,[9−14] the large amount of z and cubic structural character significantly influence the electrochemical reactivity. We, thus, examined the electrochemical reactivity of the $x = 0.75$ samples prepared using the NaCl and KCl flux media. Figure 11 shows the charge

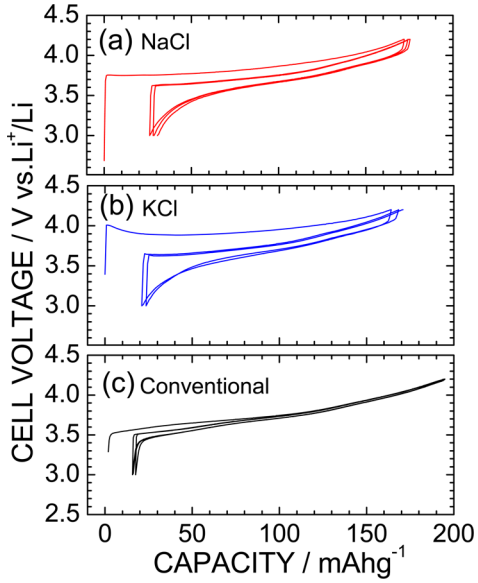

Figure 11. Charge and discharge curves for the $Li/LiCo_{1-x}Ni_xO_2$ cells with $x = 0.75$ prepared in (a) NaCl and (b) KCl media. (c) Charge and discharge curves for the conventional $x = 0.75$ sample shown for comparison.

and discharge curves for the $Li/LiCo_{1-x}Ni_xO_2$ cells with $x = 0.75$ prepared in the (a) NaCl and (b) KCl media. The charge and discharge curves for both samples significantly differ from those for the conventional $x = 0.75$ sample (see Figure 10c). For instance, the V_{cell} values at the beginning of the charge reaction rapidly increase to ~3.8 V for NaCl and ~4.0 V for KCl, while that is ~3.5 V for the conventional $x = 0.75$ sample. It is empirically known that the charge and discharge curves at the initial cycle are different from those at the subsequent

cycles, due to the decomposition reaction between active material (or lithium metal) and electrolyte.[28] Here the samples prepared using the NaCl and KCl flux media were washed with distilled water after the synthesis. Thus, the rapid increase in V_{cell} at the beginning of the charge reaction is probably attributed to the decomposition reaction between the adsorbed water on the sample and electrolyte, as in the case for the chemically delithiated Li_xNiO_2 compound.[29] Besides of the difference at the initial cycle, the hysteresis between the charge and discharge curves, i.e., the polarization for the NaCl and KCl samples is larger than that for the conventional $x = 0.75$ sample. The polarization for both samples is ~0.4 V at the middle point of the charge and discharge curves, whereas that for the conventional $x = 0.75$ sample is less than 0.05 V. This is caused by the difference in crystal structure between the samples, as clarified by the Rietveld analyses; the large amount of z hinders the diffusion of the Li^+ ions, because the rock-salt phase $(Li_{1-z}Ni_z)_{3b}[Co_{1-x}Ni_{x-z}]_{3a}O_2$ ($Fm\bar{3}m$) with $z > \sim 0.1$ is electrochemically inactive. As a results, the Q_{gra} values are 146 mAh g^{-1} for NaCl and 145 mAh g^{-1} for KCl, which are ~33 mAh g^{-1} less than that for the conventional $x = 0.75$ sample.

As described above, we have a dilemma concerning high d_p and high W_{vol} values on the $x = 0.75$ sample. The actual W_{vol} value for the conventional $x = 0.75$ sample was decreased, due to the smaller value for d_p (~4.6 g cm^{-3}) as compared with d_{XRD} [= 4.871(1) g cm^{-3}]. The high d_p values (~4.8 g cm^{-3}) were obtained by the flux method, but the flux method also induced the structural changes on z and $I(003)/I(104)$. Therefore, the Q_{gra} values, i.e., the W_{vol} values for the samples prepared with the flux method were less than that for the conventional $x = 0.75$ sample. The situation for the $x > 0.75$ samples is though to be similar to that for the $x = 0.75$ sample, because the amount of z increases with x (section 3.1). Although the optimum synthetic condition for obtaining both high d_p and high W_{vol} values is currently unknown, the results on the $Li(Ni_{0.8}Co_{0.1}Mn_{0.1})O_2$ compounds[21] would provide crucial information to overcome such dilemma. As described above, the $Li(Ni_{0.8}Co_{0.1}Mn_{0.1})O_2$ compound prepared with the NaCl flux medium indicated high d_p value close to d_{XRD} and the cubic structural character in terms of the $I(003)/I(104)$ value. Nevertheless, the charge and discharge curves for such compound are almost similar to those for the conventional $Li(Ni_{0.8}Co_{0.1}Mn_{0.1})O_2$ compound, which has almost perfect layered structure.[21] Although the origin of the difference behavior of $LiCo_{0.25}Ni_{0.75}O_2$ and $Li(Ni_{0.8}Co_{0.1}Mn_{0.1})O_2$ is currently unclear, it is expected that the existence of the Mn ions in the Li layer should affect their electrochemical properties. This is because the Q_{gra} value for the $LiNi_{1/2}Mn_{1/2}O_2$ compound is ~200 mAh/g, although its $I(003)/I(104)$ value indicates the presence of the Mn ions in the Li layer.[15] The present study focused on the x dependences of d_p, d_{XRD}, W_{vol} for the solid solution samples $LiCo_{1-x}Ni_xO_2$ with $0 \le x \le 1$. Further density measurements of $LiCo_{1-x-y}Ni_xMn_yO_2$ associated their Q_{gra}, Q_{vol}, and W_{vol} would offer essential information for increasing actual W_{vol} of LIBs.

4. CONCLUSION

The volumetric energy density W_{vol} is one of the most important parameters for high-energy density lithium-ion batteries (LIBs). A systematic study of Q_{gra}, Q_{vol}, W_{vol}, d_p, and d_{XRD} for the $LiCo_{1-x}Ni_xO_2$ samples with $0 \le x \le 1$ was performed in order to clarify the factors affecting the W_{vol}. The x dependence of Q_{gra}, Q_{vol}, and W_{vol} was divided into three distinct regions. For instance, the value of W_{vol} calculated using d_p slightly decreased from 2720 mWh cm^{-3} for $x = 0$ to 2479 mWh cm^{-3} for $x = 0.25$, then rapidly increased to 2797 mWh cm^{-3} for $x = 0.667$ with a change in the slope (dW_{vol}/dx), and finally reached a maximum (= 3268 mWh cm^{-3}) for $x = 0.9$. Because the structural parameters, including a_h, c_h, and V_h, decreased linearly with x, d_{XRD} monotonically decreased from 5.062(1) g cm^{-3} for $x = 0$ to 4.779(1) g cm^{-3} for $x = 1$. On the contrary, the x dependence of d_p was not monotonic. That is, d_p decreased almost linearly in the x range between 0 and 0.5, then d_p rapidly dropped to 4.63(2) g cm^{-3} at $x > 0.5$, and finally leveled off to a constant value (~4.60 g cm^{-3}) with further increasing x. Cross-sectional observations revealed that significantly lower values for d_p as compared to d_{XRD}, particularly for $x > 0.5$, is attributed to the presence of closed pores in agglomerated secondary particles. Therefore, the actual W_{vol} decreases from the ideal W_{vol}, particularly for $x > 0.5$, because of the presence of closed pores in secondary particles. In other words, the synthesis of well-developed primary particles without closed pores is essential for increasing the actual W_{vol}. The synthesis of a sample with well-developed primary particles was thus attempted using NaCl or KCl as a flux medium. Although high d_p values were obtained for the $x = 0.75$ samples prepared in this manner, a structural change from the hexagonal phase to cubic phase was also induced. Hence, the values of Q_{gra} for such samples were less than that for the conventional sample. Although it seem that current LIBs rely on electrode packing technologies, these results suggest that a deeper understanding of the differences between d_{ele} and d_p (or d_{XRD}) would offer crucial information for the development of high-energy density LIBs.

■ ASSOCIATED CONTENT

Supporting Information

Schematic illustration of the gas pycnometer system, d_p for the $x = 0$ sample as a function of each measurement, XRD patterns for the $x = 0.05$, 0.1, 0.333, 0.667, 0.9, and 0.95 samples, the Rietveld analyses for the $x = 0.9$, 0.95, and 1 samples, charge and discharge curves for the $Li/LiCo_{1-x}Ni_xO_2$ cells with $x = 0.05$, 0.1, 0.333, 0.667, 0.9, and 0.95, and the average operating voltage for the $LiCo_{1-x}Ni_xO_2$ samples. This material is available free of charge via the Internet at http://pubs.acs.org.

■ AUTHOR INFORMATION

Corresponding Author

*E-mail: e1089@mosk.tytlabs.co.jp. Phone: +81-561-71-7698. Fax: +81-561-63-6156.

Notes

The authors declare no competing financial interest.

■ ACKNOWLEDGMENTS

We thank Mrs. Y. Kumai and Mr. Y. Akimoto of TCRDL for assistance with d_p measurements and cross-sectional SEM observations, respectively. This study was partially supported by a Grant-in-Aid for Scientific Research (C), 25410207, from the Ministry of Education, Culture, Sports, Science, and Technology, Japan.

■ REFERENCES

(1) Nazri, G.-A.; Pistoia, G. *Lithium Batteries: Science and Technology*; Kluwer Academic: Dordrecht, The Netherlands, 2004.

(2) Dahn, J. R.; Ehrlich, G. E. In *Linden's Handbook of Batteries*, fourth ed.; Reddy, T. B., Eds.; McGraw-Hill: New York, 2011; Chapter 26, pp 26.1−26.79.
(3) Mizushima, K.; Jones, P. C.; Wiseman, P. J.; Goodenough, J. B. Li_xCoO_2 ($0 < x < 1$): A New Cathode Material for Batteries of High Energy Density. *Mater. Res. Bull.* **1980**, *15*, 783−789.
(4) Reimers, J. N.; Dahn, J. R. Electrochemical and In Situ X-Ray Diffraction Studies of Lithium Intercalation in Li_xCoO_2. *J. Electrochem. Soc.* **1992**, *139*, 2091−2097.
(5) Ohzuku, T.; Ueda, A. Solid-State Redox Reactions of $LiCoO_2$ ($R\bar{3}m$) for 4 V Secondary Lithium Cells. *J. Electrochem. Soc.* **1994**, *141*, 2972−2977.
(6) Mukai, K.; Kishida, K.; Nozaki, H.; Dohmae, K. Structural Phase Transition from Rhombohedral ($R\bar{3}m$) to Monoclinic (C2/m) Symmetry in Lithium Overstoichiometric $Li_{1+\delta}Co_{1-\delta}O_{2-\delta}$. *Chem. Mater.* **2013**, *25*, 2828−2837.
(7) Mukai, K.; Aoki, Y.; Andreica, D.; Amato, A.; Watanabe, I.; Giblin, S. R.; Sugiyama, S. Thermally Activated Spin Fluctuations in Stoichiometric $LiCoO_2$ Clarified by Electron Paramagnetic Resonance and Muon-Spin Rotation and Relaxation Measurements. *Phys. Rev. B* **2014**, *89*, 094406.
(8) Dahn, J. R.; von Sacken, U.; Michal, C. A. Structure and Electrochemistry of $Li_{1\pm y}NiO_2$ and a New Li_2NiO_2 Phase with the $Ni(OH)_2$ Structure. *Solid State Ionics* **1990**, *44*, 87−97.
(9) Ohzuku, T.; Ueda, A.; Nagayama, M. Electrochemistry and Structural Chemistry of $LiNiO_2$ ($R\bar{3}m$) for 4 V Secondrary Lithium Cells. *J. Electrochem. Soc.* **1993**, *140*, 1862−1870.
(10) Delmas, C.; Saadoune, I. Electrochemical and Physical Properties of the $Li_xNi_{1-y}Co_yO_2$ Phase. *Solid State Ionics* **1992**, *53*−*56*, 370−375.
(11) Ohuzku, T.; Ueda, A.; Nagayama, M.; Iwakoshi, Y.; Komori, H. Comparative Study of $LiCoO_2$, $LiNi_{1/2}Co_{1/2}O_2$ and $LiNiO_2$ for 4 V Secondary Lithium Cells. *Electrochim. Acta* **1993**, *38*, 1159−1167.
(12) Saadoune, I.; Delmas, C. $LiNi_{1-y}Co_yO_2$ Positive Electrode Materials: Relationships between the Structure, Physical Properties and Electrochemical Behaviour. *J. Mater. Chem.* **1996**, *6*, 193−199.
(13) Mukai, K.; Sugiyama, J.; Ikedo, Y.; Brewer, J. H.; Ansaldo, E. J.; Morris, G. D.; Ariyoshi, K.; Ohzuku, T. Microscopic Magnetism in Lithium Insertion Materials of $LiNi_{1-x}Co_xO_2$ (x = 0, 1/4, 1/2, 3/4, and 1). *J. Power Sources* **2007**, *174*, 843−846.
(14) Mukai, K.; Sugiyama, J.; Aoki, Y. Structural, Magnetic, and Electrochemical Studies on Lithium Insertion Materials $LiNi_{1-x}Co_xO_2$ with $0 \leq x \leq 0.25$. *J. Solid State Chem.* **2010**, *183*, 1726−1732.
(15) Ohzuku, T.; Ariyoshi, K.; Makimura, Y.; Yabuuchi, N.; Sawai, K. Materials Strategy for Advanced Lithium-Ion (Shuttlecock) Batteries: Lithium Nickel Manganese Oxides with or without Cobalt. *Electrochemistry* **2005**, *73*, 2−11.
(16) Ohzuku, T.; Ueda, A. Why Transition Metal (Di)oxides Are the Most Attractive Materials for Batteries. *Solid State Ionics* **1994**, *69*, 201−211.
(17) Islam, M. S.; Fisher, C. A. J. Lithium and Sodium Battery Cathode Materials: Computational Insights into Voltage, Diffusion and Nanostructural Properties. *Chem. Soc. Rev.* **2014**, *43*, 185−204.
(18) Lowell, S.; Shields, J. E.; Thomas, M. A.; Thommes, M. *Characterization of Porous Solids and Powders: Surface Area, Pore Size and Density*; Kluwer Academic: Dordrecht, The Netherlands, 2004.
(19) Hosoya, M.; Ikuta, H.; Wakihara, M. Single Phase Region of Cation Substituted Spinel $LiM_yMn_{2-y}O_{4-\delta}$ (M = Cr, Co and Ni) and cathode property for lithium secondary battery. *Solid State Ionics* **1998**, *111*, 153−159.
(20) Hayashi, N.; Ikuta, H.; Wakihara, M. Cathode of $LiMg_yMn_{2-y}O_4$ and $LiMg_yMn_{2-y}O_{4-\delta}$ Spinel Phases for Lithium Secondary Batteries. *J. Electrochem. Soc.* **1999**, *146*, 1351−1354.
(21) Kim, Y. Lithium Nickel Cobalt Manganese Oxide Synthesized Using Alkali Chloride Flux: Morphology and Performance As a Cathode Material for Lithium Ion Batteries. *ACS Appl. Mater. Interfaces* **2012**, *4*, 2329−2333.
(22) Izumi, F.; Ikeda, T. A Rietveld-analysis Program RIETAN-98 and Its Applications to Zeolites. *Mater. Sci. Forum* **2000**, *321*−*324*, 198−203.
(23) Shannon, R. D.; Prewitt, C. T. Effective Ionic Radii in Oxides and Fluorides. *Acta Crystallogr., Sect. B* **1969**, *B25*, 925−946.
(24) Ohzuku, T.; Ueda, A. Phenomenological Expression of Solid-State Redox Potentials of $LiCoO_2$, $LiCo_{1/2}Ni_{1/2}O_2$, and $LiNiO_2$ Insertion Electrodes. *J. Electrochem. Soc.* **1997**, *144*, 2780−2785.
(25) Kim, Y.; Lee, H.; Kang, S. First-Principles and Experimental Investigation of the Morphology of Layer-Structured $LiNiO_2$ and $LiCoO_2$. *J. Mater. Chem.* **2012**, *22*, 12874−12881.
(26) Teshima, K.; Lee, S.; Mizuno, Y.; Inagaki, H.; Hozumi, M.; Kohama, K.; Yubuta, K.; Shishido, T.; Oishi, S. Environmentally Friendly Growth of Well-Developed $LiCoO_2$ Crystals for Lithium-Ion Rechargeable Batteries Using a NaCl Flux. *Cryst. Growth Des.* **2010**, *10*, 4471−4475.
(27) Teshima, K.; Inagaki, H.; Tanaka, S.; Yubuta, K.; Hozumi, M.; Kohama, K.; Shishido, T.; Oishi, S. Growth of Well-Developed $Li_4Ti_5O_{12}$ Crystals by the Coolign of a Sodium Chloride Flux. *Cryst. Growth Des.* **2011**, *11*, 4401−4405.
(28) Mukai, K.; Sugiyama, J.; Ikedo, Y.; Nozaki, H.; Kamazawa, K.; Andreica, D.; Amato, A.; Månsson, M.; Brewer, J. H.; Ansaldo, E. J.; Chow, K. H. Micrscopic Magnetic Study on the Nominal Composition $Li[Li_{1/3}Mn_{5/3}]O_4$ by Muon-Spin Rotation/Relaxation Measurements. *J. Phys. Chem. C* **2010**, *114*, 11320−11327.
(29) Mukai, K.; Sugiyama, J.; Ikedo, Y.; Aoki, Y.; Andreica, D.; Amato, A. Structural and Magnetic Nature for Fully Delithiated Li_xNiO_2: Comparative Study between Chemically and Electrochemically Prepared Samples. *J. Phys. Chem. C* **2010**, *114*, 8626−8632.